JOURNAL OF SOLID STATE CHEMISTRY 42, 242–250 (1982)

Growth and Physical Properties of Single Crystals of $Fe_2^{II}Mo_3^{IV}O_8$

P. STROBEL, Y. LE PAGE, AND S. P. McALISTER

Solid State Chemistry, National Research Council of Canada, Ottawa, Ontario K1A 0R9, Canada

Received October 23, 1981; in final form December 21, 1981

Crystals of hexagonal $Fe_2Mo_3O_8$ up to 3 × 3 × 2 mm were grown by chemical vapor transport from a starting mixture of composition Fe_2MoO_4. The morphology is {101}, {10$\bar{2}$}, {110}, {00$\bar{2}$}, {100} and corresponds to the absolute orientation of the polar z axis. Both magnetic susceptibility and electrical conductivity show considerable anisotropy. The compound orders antiferromagnetically at 59.5 K, with the spin along c. It is a low-conductivity semiconductor with activation energies 0.14 and 0.21 eV perpendicular and parallel to c, respectively.

Introduction

Iron (II) and molybdenum(IV) form two mixed oxides: $Fe_2Mo_3O_8$, first synthesized by McCarroll *et al.* (*1*), and the spinel-type Fe_2MoO_4, found by Rahmel *et al.* (*2*). A third phase of formula $FeMoO_3$, reported by Rusakov *et al.* (*3*), was not found in a more recent phase study (*4*) and was probably $Fe_2Mo_3O_8$ (*5*). These mixed oxides, which are believed to play an important role in the properties of molybdenum steels (*2, 3*), exhibit interesting magnetic properties. $Fe_2Mo_3O_8$ is a hexagonal compound containing diamagnetic (Mo_3) clusters which orders antiferromagnetically at 59 ± 3 K (*6, 7*), whereas Fe_2MoO_4 exhibits a weak spontaneous magnetization below 348 K, with an unexplained change of sign at 160 K (*8*). Little is known about the electrical properties of these compounds.

The purpose of the present study is to investigate some physical properties of iron(II)–molybdenum(IV) oxides in single-crystal form. The crystal growth of these materials is beset by numerous problems. Growth from the liquid phase is not feasible, because of the lack of data about solid–liquid phase equilibria and thermodynamics of the Fe–Mo–O system. Growth from the vapor by the chemical transport technique has been applied to both molybdenum dioxide (*9–11*) and iron oxides (*12–14*), using various transporting agents. In the latter case, Fe_2O_3 and Fe_3O_4 are easily transported, but not FeO. According to Emmenegger (*14*), iron monoxide reacts so strongly with silica glass at 850–1000°C that proper transport does not occur. In a recent study of iron(II) mixed oxides grown by chemical vapor transport, an inner coating of the silica tube with carbon provided an effective protection, at least at temperatures up to ~930°C (*15*).

We report here the growth of single crystals of Fe(II)–Mo(IV) oxides. Large crystals of $Fe_2Mo_3O_8$ were obtained, and their morphology, as well as their magnetic and electrical properties, are described.

0022-4596/82/060242-09$02.00/0

Experimental

Single-crystal preparation. The crystal growth was carried out using the chemical vapor transport technique. The starting materials were dry reagent-grade Fe, Fe_2O_3 (Fisher Co.), and MoO_2 (Alfa Inorganics). The actual iron metal content of the iron powder was checked titrimetrically and found to be $98.9 \pm 0.3\%$. The starting materials were introduced directly into the transport tubes. The following transporting agents were tried: Cl_2 (99.9%, Matheson Co.), HCl (99.0%, Matheson Co.), and $TeCl_4$, introduced in the transport tubes as high-purity Te (Johnson–Mathey Co.) plus gaseous Cl_2.

Crystals were grown in evacuated silica tubes (10–15 mm in diameter, 150–200 mm long) using a two-zone furnace. The growth zone was cleaned *in situ* by a back-transport process for 20 hr. After thermal equilibrium was established in the tube, the transport was allowed to proceed by slowly decreasing the growth zone temperature (~2°C/hr). The crystals were easily detached from the tube walls and washed in dilute hydrochloric acid. No evidence of oxidation of Fe(II)–Mo(IV) oxides was found for clean crystal surfaces on contact with air or water.

Measurement procedures. The crystals were identified and oriented using a 4-circle X-ray diffractometer with Mo$K\alpha$ radiation. Their morphology was determined by optical goniometry on the diffractometer, using a projector and a telescope symmetrically arranged about the diffraction vector so that the planes brought into a diffraction position give optical reflections similar to those obtained in a 2-circle goniometer.

The magnetization in a 22-mg oriented single crystal of $Fe_2Mo_3O_8$ was measured in the range 4.2–300 K using a vibrating-sample magnetometer. Measurements were made with the applied field along the crystallographic z axis and perpendicular to it. The shape of the sample was not spherical, but sufficiently regular for there to be no significant shape anisotropy.

Resistivity measurements on $Fe_2Mo_3O_8$ were not possible using the usual Van der Pauw technique (*16*), due to the large anisotropy in resistance observed in a non-oriented single-crystal plate. Instead, a plate containing the hexagonal z axis was cut from a single crystal and polished down to a thickness of 0.31 mm. It was separated into two samples for measurements parallel and perpendicular to z. Two-probe arrangements were used due to the small size of the final samples. We believe that the contact resistance was negligible in the range of resistances measured (10^6 to 10^{10} Ω). The contacts were ohmic up to ~1 V potential drop across the samples. The voltages were measured using a high-impedance electrometer (Keithley Model 616, input impedance 10^{14} Ω).

Results and Discussion

1. Crystal Growth

The experimental conditions and results of chemical vapor transport are summarized in Table I. The cubic crystals were spinel-type $Fe_{2+x}Mo_{1-x}O_4$, with cell parameters intermediate between the ones reported for Fe_3O_4 and Fe_2MoO_4 (*17*). Table I shows that chemical vapor transport from a starting mixture with a molar ratio Fe/Mo = 2 (i.e., aiming at Fe_2MoO_4) produced crystals with Fe/Mo ratios either <2 ($Fe_2Mo_3O_8$) or >2 (spinel phase). The transport tubes were heavily attacked at temperatures >1000°C (runs A and B). Crystals were grown successfully by reducing the temperature and using double-tubing to prevent admission of atmospheric oxygen into cracked tubes. No improvement was found when tubes coated with carbon were used. Both the quality and composition of the crystals varied with the nature of the trans-

TABLE I

EXPERIMENTAL CONDITIONS AND RESULTS OF CHEMICAL VAPOR TRANSPORT

Run	Starting ratio FeO^a/MoO_2	Transport agent	Temperatures charge/growth (°C)	Duration (days)	Results
A	1.98	Cl_2 175 Torr	1068/1025	24	Heavy attack, no crystals
B	2.00	HCl 50 Torr	1068/1025	24	Heavy attack, $Fe_2Mo_3O_8$ + spinel crystals
C	2.04	HCl 50 Torr	958/853	19	Spinel crystals, very small transported amount
D	1.91	$TeCl_4$ 1.45 g/liter	958/853	19	Large $Fe_2Mo_3O_8$ crystals

[a] As Fe_2O_3 + Fe.

porting agent. Best results, which were obtained using $TeCl_4$ in the temperature range 850–960°C (run D), produced shiny black crystals of $Fe_2Mo_3O_8$ up to 3 × 3 × 2 mm (see Figs. 1 and 2).

The difference in chemical composition between the charge and the crystals can be understood by taking into account the strong reactivity of Fe^{2+} compounds with silica, the high-temperature properties of the Fe–Mo–O system, and the thermodynamics of the chemical transport. It follows from the reaction of iron with the container that (i) Fe^{2+} ions are trapped on the silica tube walls where they form nonvolatile silicates, leading to a decrease of the Fe/Mo ratio in the growth zone, and (ii) some oxygen is introduced by reactions involving H_2O adsorbed on the tube walls and by diffusion through attacked tubes. (Oxygen must be present for the formation of the nonstoichiometric spinel phase, where the substitution of x Mo by x Fe is accompanied by the oxidation of $2x$ Fe^{2+} to Fe^{3+}.)

The simultaneous deposition of $Fe_2Mo_3O_8$ and $Fe_{2+x}Mo_{1-x}O_4$ in run B is in agreement with the results of a high-temperature phase

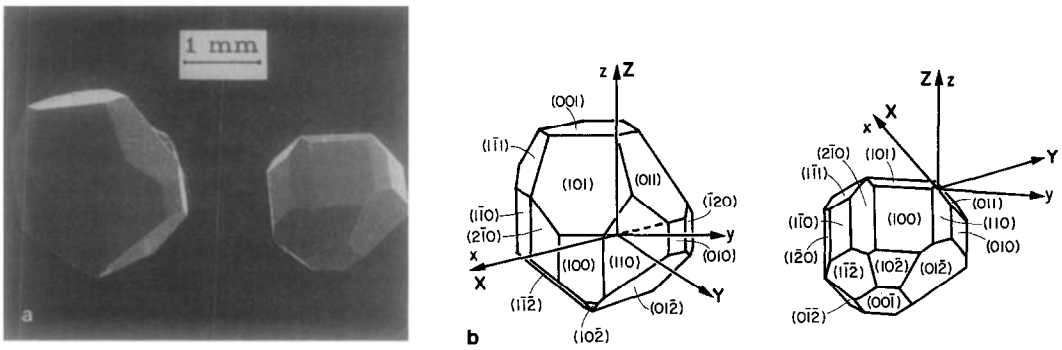

FIG. 1. Equidimensional crystals of $Fe_2Mo_3O_8$: (a) SEM photograph, (b) face indices. The crystallographic system of coordinates *xyz* and the physical system *XYZ* according to the IRE rules (*21*) are shown.

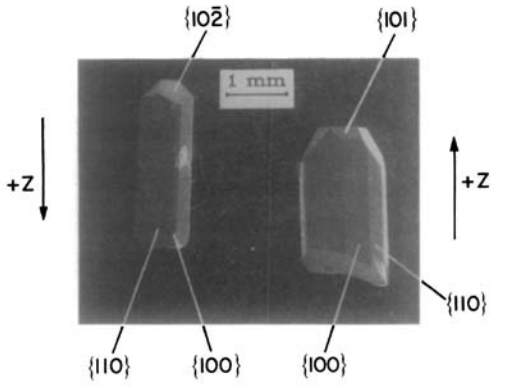

FIG. 2. Prismatic crystals of $Fe_2Mo_3O_8$. The crystal forms and the absolute sense of the z axis are shown.

study by Abe (*4*), who showed that there are only two ternary solid phases in the Fe(II or III)–Mo(IV)–O system at 1140°C: $Fe_2Mo_3O_8$, with no significant solid solution range, and a spinel phase with a continuous range of compositions from Fe_3O_4 to Fe_2MoO_4. In addition, Abe showed that stoichiometric Fe_2MoO_4 is much more sensitive to oxidation than $Fe_2Mo_3O_8$, the upper limit of their equilibrium oxygen pressures at 1140°C being $10^{-11.8}$ and $10^{-8.3}$ atm, respectively. Between these two limiting pressures, Fe_2MoO_4 is converted into a mixture of $Fe_2Mo_3O_8$ and a partially oxidized spinel phase, as observed in the chemical transport in run C. Thus the nature and composition of the phases obtained are directly related to the oxygen pressure in the transport tube, as shown by the overall reaction:

$$(4 + 5x)\text{“}Fe_2MoO_4\text{”} + 2xO_2 \rightarrow 4Fe_{2+x}Mo_{1-x}O_4 + 3xFe_2Mo_3O_8.$$

The influence of the transporting agent is illustrated by the transport reactions given in Table II. It must be emphasized that this set of reactions is a very simplified description of the chemical equilibria involved. In a complex system such as MoO_2–$TeCl_4$, where various oxychlorides are formed, only the reaction involving $MoOCl_2$ is given, since this compound has been found to be the main Mo-containing constituent in the vapor phase (*11*). It can be seen from the thermodynamic functions for these reactions (computed for 1200 K in Table II) that the free enthalpy of reaction is larger for MoO_2 than for FeO in the presence of HCl, and conversely with “$TeCl_4$” (which consists mostly of $TeCl_2 + Cl_2$ at 1200 K); this favors lower Fe/Mo ratios in the latter case. On the other hand, the transport

TABLE II

THERMODYNAMIC FUNCTIONS[a] FOR TYPICAL TRANSPORT REACTIONS OF FeO AND MoO_2 AT 1200 K (ALL CONSTITUENTS GASEOUS, EXCEPT s = SOLID)

	ΔH (kcal/mole)	ΔS (cal/K · mole)	ΔG (kcal/mole)
$FeO(s) + 2\,HCl \rightarrow FeCl_2 + H_2O$	+12.6	+ 7.3	+ 3.9
$MoO_2(s) + 2\,HCl \rightarrow MoO_2Cl_2 + H_2$	+36.5	+11.3	+22.9
modified by $x\,H_2 + \frac{x}{2}\,O_2 \rightarrow x\,H_2O$	$-59.5x$	$-13.4x$	$-43.4x$
$FeO(s) + (TeCl_2 + Cl_2) \rightarrow FeCl_2 + TeOCl_2$	− 1.8	+ 5.4	− 8.3
$MoO_2(s) + \frac{1}{2}(TeCl_2 + Cl_2) \rightarrow MoOCl_2 + \frac{1}{4}Te_2$	+ 8.6	+19.4	−14.7
modified by $\frac{x}{4}\,Te_2 + \frac{x}{2}\,O_2 \rightarrow \frac{x}{2}\,TeO_2$	$-17.3x$	$-6.4x$	$-9.5x$

[a] Data drawn from Refs. *11* (oxychlorides) and *18* (all other phases).

reactions of MoO_2 involve reduced species such as H_2 or Te_2. They are therefore very sensitive to oxygen, which will enhance the transport by HCl.

We thus conclude that stoichiometric Fe_2MoO_4 can probably not be obtained by chemical vapor transport in silica tubes, because of the incompatibility between a very low equilibrium oxygen pressure and the oxidizing effect of the reaction with silica; $Fe_2Mo_3O_8$ grows because of a shift in composition due to the reaction with silica and the preferential transport of Mo in the presence of $TeCl_4$. Only $Fe_2Mo_3O_8$ is dealt with in the following sections.

2. *Structure and Morphology of $Fe_2Mo_3O_8$ Crystals*

The structure of $Fe_2Mo_3O_8$ was first described by McCarroll *et al.* (*1*). The crystals obtained here are hexagonal, space group $P6_3mc$, with cell parameters $a = 5.7732(6)$ and $c = 10.054(1)$ Å at 25°C, as established in a recent structure refinement (*5*). The structure contains close-packed oxygen ions, with alternate Mo- and Fe-containing planes perpendicular to the z axis (see Fig. 3). The Mo layers contain Mo_3 clusters with Mo–Mo distances 2.530 Å (3.244 Å with adjacent clusters). The iron layers contain two different sites, Fe 1 and Fe 2, tetrahedrally and octahedrally coordinated with oxygen, respectively. The Fe 1 and Fe 2 sites have slightly different z coordinates, thus forming two mutually centering triangular patterns displaced by 0.614 Å along z with respect to each other. Each Fe 1 has three nearest iron neighbors Fe 2 in the same layer at 3.389 Å (and vice versa). The second iron nearest neighbor of Fe 1 is an Fe 2 in an adjacent layer at 4.413 Å along z. All the FeO_4 tetrahedra at Fe 1 have a corner pointing toward the positive direction of the z axis. This structural feature illustrates the polar nature of the z axis in point group $6mm$, which results in polar properties such as pyroelectricity.

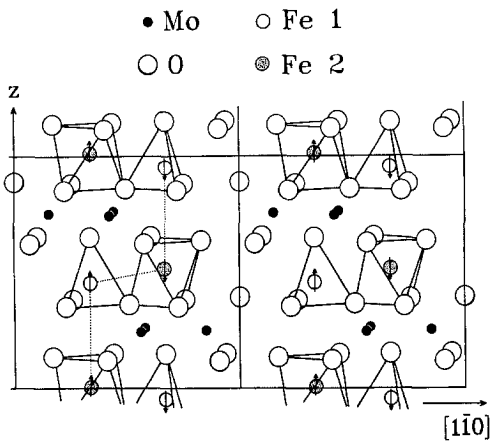

FIG. 3. Projection of the structure of $Fe_2Mo_3O_8$ on a (110) plane (z axis vertical). The coordination polyhedra of the iron ions only are shown. The dotted lines show shortest Fe–Fe distances (in an Fe layer) and second shortest Fe–Fe distances (parallel to z). The arrows indicate the proposed spin orientation in the antiferromagnetic phase (see text).

Although the positive sense of the z axis is defined at the atomic level, it is difficult to find its orientation by X-ray diffraction because there is a symmetry center at the origin of reciprocal space in the absence of anomalous scattering (Friedel's law). To establish the sense of the polar axis, it should be referred to a simple structure-related macroscopic property which distinguishes its extremities. These considerations, as well as the quality of the crystals, prompted a morphological study of $Fe_2Mo_3O_8$ crystals.

Two different habits were observed: some crystals were rather equidimensional (Fig. 1), and others were prismatic and elongated (Fig. 2). The morphological study showed that they consist of the same forms, but with different developments. In the equidimensional crystals, the ranking by decreasing face development is $\{101\}$, $\{10\bar{2}\}$, $\{110\}$, $\{00\bar{2}\}$, $\{002\}$, $\{100\}$. In the prismatic crystals, the hexagonal prisms $\{110\}$ and $\{100\}$ become predominant, the other forms keeping their relative development. According to the Donnay–Harker law (*19*),

TABLE III

MEASURED AND CALCULATED BIJVOET RATIOS FOR THREE REFLECTIONS IN $Fe_2Mo_3O_8$

Reflection indices		407	802	737
Bijvoet ratios	Crystal 1	0.88 (1)	1.14 (2)	0.75 (4)
	Crystal 2	0.852 (5)	1.16 (1)	0.78 (2)
	Calculated (from Ref. 5)	0.859	1.167	0.769

these forms, together with $\{10\bar{1}\}$ and $\{102\}$, should be the most frequently occurring faces. However, the forms $\{10\bar{1}\}$ and $\{102\}$ were absent in all the doubly terminated crystals we examined (about 50). The different nature of the truncated hexagonal pyramids $\{101\}$ or $\{10\bar{2}\}$ terminating the crystals thus provides a simple way to distinguish the extremities of the crystals along z, i.e., to identify the absolute sense of the polar axis.

The morphology–structure relation was determined using Bijvoet ratios (*20*). The list of structure factors in $Fe_2Mo_3O_8$ (*5*) gives several Bijvoet ratios significantly different from 1 for Mo radiation. Three such ratios were measured on two crystals: a very small crystal A to minimize absorption effects (dimensions $30 \times 30 \times 100$ μm), and a $100 \times 100 \times 150$-$\mu$m crystal B. Crystal A was singly terminated and its termination was identified visually under a microscope. Crystal B was doubly terminated and its morphology was checked optically on the diffractometer. Both crystals were oriented with the crystallographic z axis pointing in the same sense as the $\{101\}$ pyramid. (The Bijvoet ratios measured here are ratios of the averages of all the reflection intensities equivalent to the *hkl* and $hk\bar{l}$ reflections.) The results (Table III) show unambiguously that this is the correct absolute sense of the z axis. Therefore the Fe 1 tetrahedra point toward the same direction as the $\{101\}$ pyramid. A procedure for the selection of the physical reference system *XYZ* according to the IRE rules (*21*) is given in the Appendix.

3. *Magnetic Properties*

The temperature variation of the magnetic susceptibility of a single crystal of $Fe_2Mo_3O_8$ is shown in Fig. 4, with field directions parallel and perpendicular to the z direction. The room-temperature magnetization varied linearly with the field in both orientations, characteristic of a paramagnetic state, but showed appreciable anisotropy. This anisotropy also revealed itself as a sinusoidal variation of M with angular deviation from the c direction.

Figure 4 shows that $Fe_2Mo_3O_8$ orders magnetically at 59.5 ± 0.5 K, in agreement with (*7*). The rapid rise in M for increasing temperature for $H \| c$ contrasts with its variation for $H \perp c$. This, together with the weak nonlinear field dependence of M at 4.2 K, indicates that the ordering is antiferromagnetic with the spin axis along the c direction. The nearest neighbors of a given ion Fe 1 belong to the Fe 2 triangular pattern in the same layer (see Section 2) and must have opposite spin orientations via direct magnetic coupling. The next nearest neighbor of Fe 1 is a Fe 2 ion located directly above

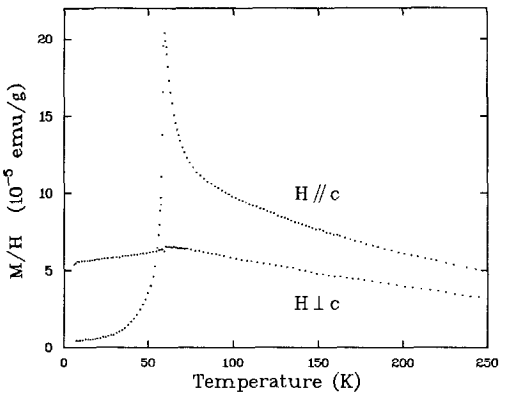

FIG. 4. Temperature dependence of the magnetic susceptibility of a single crystal of $Fe_2Mo_3O_8$ for fields parallel and perpendicular to the c direction. The applied field was 15 kOe $H \| c$ and 5 kOe for $H \perp c$.

(or below) Fe 1 along c (Fig. 3). In this case, the magnetic coupling is indirect because of the intervening Mo and O layers, and it could be either ferromagnetic or antiferromagnetic.

Although the paramagnetic moment is generally obtained through a plot of χ^{-1} or M^{-1} vs T, it is often useful to write the exact expression for χ^{-1} as

$$\chi^{-1} = \frac{T}{C}\left(1 + \sum_{n=1}^{\infty} \frac{\lambda_n}{T^n}\right),$$

where C is the Curie constant and λ_n are functions of the moments at the lattice sites and their interactions (*22*). (This expression reduces to the Curie–Weiss law if the terms for $n > 1$ are omitted.) A plot of $(\chi T)^{-1}$ vs T^{-1} then yields the Curie constant as an intercept; the slope of the plot reflects the dominant coupling between the magnetic ions, and the low-temperature scale is expanded (*23*). Plots of $Q = (\chi T)^{-1}$ vs T^{-1} with $H \| c$ and $H \perp c$ are shown in Fig. 5 for an applied field of 15 kOe. From this and a similar plot at 5 kOe, we obtain the following effective magnetic moments:

for $H \| c$: $\mu_{\text{eff}} = 5.8 \pm 0.3\ \mu_B$/Fe ion,
for $H \perp c$: $\mu_{\text{eff}} = 4.4 \pm 0.2\ \mu_B$/Fe ion.

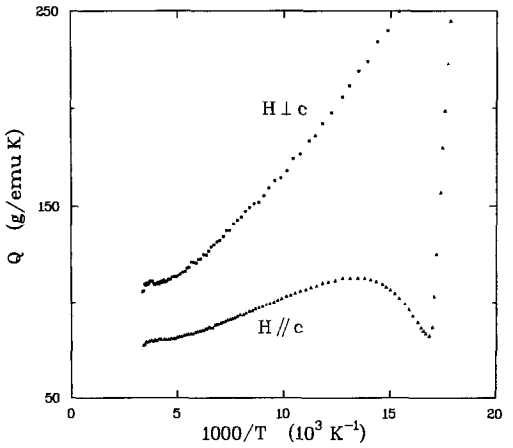

FIG. 5. Plot of $Q = (\chi T)^{-1}$ vs reciprocal temperature for fields parallel and perpendicular to c. The applied field was 15 kOe for both field orientations.

The corresponding value for a sample of random orientation is $(\frac{1}{3})(5.8) + (\frac{2}{3})(4.4) = 4.9\ \mu_B$, in excellent agreement with the spin-only magnetic moment of the Fe^{2+} ion (4.90 μ_B) and the value of 4.85 μ_B obtained on a powdered sample of $Fe_2Mo_3O_8$ by McCarroll *et al.* (*1*). Bertrand and Kerner-Czeskleba (*7*) quote an effective moment of 5.7 μ_B. Our measurements would suggest that their powder specimen contained a large number of oriented crystals. The unusual anisotropy in the effective magnetic moment shows that the magnetism is strongly influenced by the layer structure of the Fe arrangement and that higher temperatures are needed to get into a truly paramagnetic state. (Strong anisotropy in the paramagnetic regime is shown by other layer compounds, eg., Fe-intercalated TaS_2 (*24*).)

The slopes of the two curves in Fig. 5 are also significant. The positive slope for the $H \perp c$ case indicates that the magnetic interactions are predominantly antiferromagnetic when viewed in a plane perpendicular to c. This is consistent with the picture already established of antiferromagnetic coupling in the Fe layers. For H along c, the slope is positive too, but there is a change of sign as T_N is approached (at $10^3/T \sim 13$, i.e., $T \sim 75$ K). (This is similar to curve D in Fig. b of (*22*).) This suggests that, in addition to the nearest-neighbor antiferromagnetic interaction, there is a ferromagnetic interaction which becomes important just above the transition. Since the second nearest iron neighbors are located above (or below) along c, we propose that the Fe moments are aligned ferromagnetically along this axis. As a result, the spin orientation of Fe 1 with respect to Fe 2 alternates from layer to layer along c, as shown in Fig. 3. A similar magnetic structure has been suggested by Bertrand and Kerner-Czeskleba (*7*) from an analysis of powder neutron diffraction spectra at 4.2 K.

4. Electrical Properties

The results of resistivity measurements in the range 77–300 K are given in Fig. 6. The conductivity in $Fe_2Mo_3O_8$ is very anisotropic: the ratios $(\sigma\perp c)/(\sigma\|c)$ vary from ~40 at room temperature to ~300 at 150 K. The material is semiconducting in both directions; the conductivity along c could not be measured below 140 K due to resistances $> 10^{10}$ Ω. The activation energies of conductivity in the high-temperature range are 0.14 eV for $\sigma\perp c$ and 0.21 eV for $\sigma\|c$.

All these results are in qualitative agreement with the structure: both a higher conductivity and a lower activation energy are observed for conduction parallel to the Fe and Mo layers ($\perp c$). Note that the intercluster Mo–Mo distance (3.244 Å) is far in excess of the Mo–Mo distances in metallic MoO_2 (2.511 Å) (*25*). The shortest Fe–Fe distances in $Fe_2Mo_3O_8$ (3.389 Å) are also large, even when compared with cation–cation distances in other semiconducting iron(II) oxidic compounds: 3.04 Å in $Fe_{1-x}O$ (*25*), 2.97 Å in Fe_2GeO_4 (*15*).

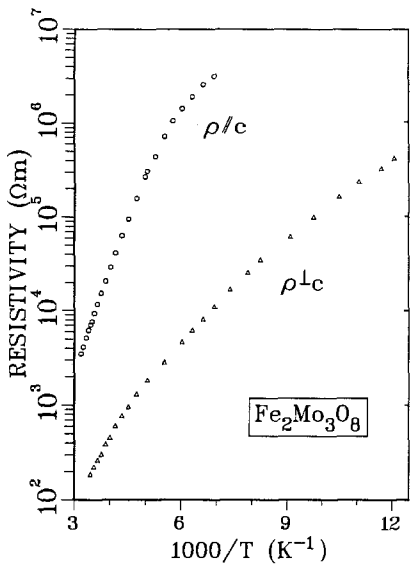

FIG. 6. The resistivity of a single crystal of $Fe_2Mo_3O_8$ as a function of temperature for currents parallel and perpendicular to c.

Given the low conductivity and the large cation–cation distances in $Fe_2Mo_3O_8$, the most likely mechanism for conduction in this material is hopping of small polarons between Fe sites. In this case, the conductivity can be written as (*26*)

$$\sigma = \frac{ne^2a^2\nu_0}{kT}\exp\left(-\frac{E_a}{kT}\right).$$

where n is the carrier density, e the charge of the electron, a the distance between hopping sites, ν_0 the phonon frequency, k the Boltzmann constant, and E_a the hopping activation energy. Thus the intercept of a $\log(\sigma T)$ vs T^{-1} plot yields $\sigma_0 = ne^2a^2\nu_0/k$. Using a typical value of $\nu_0 \sim 10^{13}$ Hz in transition metal oxides (*23*) and the intercepts $\sigma_0(\perp c) = 1050\ \Omega^{-1}\ m^{-1}$ and $\sigma_0(\|c) = 390\ \Omega^{-1}\ m^{-1}$, we obtain $n \sim 10^{17}\ cm^{-3}$ (for both directions). $Fe_2Mo_3O_8$ ($d = 6.02$ g cm^{-3} (*1*)) has an iron site density $n_{Fe} = 1.37 \times 10^{22}\ cm^{-3}$. If we assume that the hopping process is related to the presence of Fe^{3+} ions, the ratio Fe^{3+}/Fe^{2+} is 10^{-5} in our sample, confirming its purity. Finally, we estimate the mobility $\mu = \sigma/ne$ at room temperature as $\sim 10^{-4}$ and $3 \times 10^{-3}\ cm^2\ V^{-1}\ sec^{-1}$ parallel and perpendicular to c, respectively, characteristic of localized-carrier, small-polaron conduction.

Conclusion

In various attempts to grow crystals of Fe(II)–Mo(IV)–O phases, we obtained large crystals of $Fe_2Mo_3O_8$. Its particular structure, containing cations arranged in layers perpendicular to a polar six-fold axis, is reflected in the physical properties of this material in single-crystal form. Morphological investigation gives a simple criterion permitting one to identify the absolute sense of the polar axis. Both the magnetic susceptibility and the electrical conductivity are strongly anisotropic. $Fe_2Mo_3O_8$ is anti-

ferromagnetic (T_N = 59.5 K), with the moments oriented along the c direction. The electrical conductivity is larger parallel to the cation layers than perpendicular to them, and is typical of a low-mobility localized-carrier material.

Appendix

The procedure for the selection of the physical reference system XYZ according to the IRE rules (*21*) in $Fe_2Mo_3O_8$ follows: The {100} faces are the only rectangular faces of the terminated crystals (see Fig. 1). Select any such face and select Z along an edge with its positive sense toward the point of the {101} pyramid, i.e., toward the termination with the more acute pyramid. (The dihedral angle (101)–($\bar{1}$01) is 50.9° while (10$\bar{2}$)–($\bar{1}$0$\bar{2}$) is 89.7°.) X is then selected along the other edge of the face, the sense being unimportant. Y is then along the common perpendicular to X and Z, oriented so that the reference system is right-handed. The crystallographic reference system xyz is right-handed and has x and z collinear to X and Z, respectively; y is in the direction making angles of 120 and 90°, respectively, with x and z.

References

1. W. H. McCarroll, L. Katz, and R. Ward, *J. Amer. Chem. Soc.* **79,** 5410 (1957).
2. A. Rahmel, W. Jaergel, and K. Becker, *Arch. Eisenhuettenwes.* **30,** 351 (1959).
3. L. N. Rusakov, I. A. Novokhatskii, L. M. Lenev, and A. A. Savinskaya, *Dokl. Akad. Nauk SSSR* **161,** 410 (1965).
4. M. Abe, *Mater. Res. Bull.* **7,** 1443 (1972).
5. Y. Le Page and P. Strobel, *Acta Crystallogr.*, in press.
6. F. Varret, H. Czeskleba, F. Hartmann-Boutron, and P. Imbert, *J. Phys. (Orsay, Fr.)* **33,** 549 (1972).
7. D. Bertrand and H. Kerner-Czeskleba, *J. Phys. (Orsay, Fr.)* **36,** 379 (1975).
8. J. Ghose, N. Greenwood, G. Hallam, and D. Read, *J. Solid State Chem.* **11,** 239 (1974).
9. H. Schaefer, T. Grofe, and M. Trenkel, *J. Solid State Chem.* **8,** 14 (1973).
10. L. E. Conroy and L. Ben-Dor, *Inorg. Synth.* **14,** 149 (1973).
11. H. Oppermann and M. Ritschel, *Krist. Tech.* **10,** 485 (1975); M. Ritschel and H. Oppermann, *Krist. Tech.* **15,** 535 (1980).
12. H. Schaefer, "Chemical Transport Reactions," Academic Press, New York (1964).
13. R. Kershaw and A. Wold, *Inorg. Synth.* **11,** 10 (1968).
14. F. Emmenegger, *J. Cryst. Growth* **2,** 33 (1968).
15. P. Strobel, F. Koffyberg, and A. Wold, *J. Solid State Chem.* **31,** 209 (1980).
16. L. J. Van der Pauw, *Philips Res. Rep.* **13,** 1 (1958).
17. R. J. Hill, J. R. Craig, and G. V. Gibbs, *Phys. Chem. Miner.* **4,** 317 (1979).
18. O. Barin, O. Knacke, and O. Kubaschewski, "Thermochemical Properties of Inorganic Substances," Springer-Verlag, Berlin/New York (1973, 1977).
19. J. D. H. Donnay and D. Harker, *Amer. Mineral.* **22,** 446 (1937).
20. J. M. Bijvoet, *Proc. Acad. Sci. Amst.* **52,** 313 (1949).
21. Institute of Radio Engineers, *Proc. IRE* **37,** 1378 (1949).
22. A. Danielian, *Proc. Phys. Soc.* **80,** 981 (1962).
23. F. B. Koch and A. Arrott, *Bull. Amer. Phys. Soc.* **7,** 263 (1962).
24. S. S. P. Parkin and R. H. Friend, *Philos. Mag.* [Part B] **41,** 65 (1980).
25. Landolt-Börnstein, "Zahlenwerte und Funktionen," New Series, Vol. III/7b, Springer-Verlag, Berlin/New York (1975).
26. J. B. Goodenough, "Magnetism and the Chemical Bond," Interscience, New York (1963).